Macromolecular Research

Article

DOI 10.1007/s13233-019-7142-0

www.springer.com/13233 pISSN 1598-5032 eISSN 2092-7673

Polymer Compositional Ratio-Dependent Morphology, Crystallinity, Dielectric Dispersion, Structural Dynamics, and Electrical Conductivity of PVDF/PEO Blend Films

Priyanka Dhatarwal
Ram Jeewan Sengwa*

Dielectric Research Laboratory, Department of Physics, Jai Narain Vyas University, Jodhpur-342 005, India

Received January 18, 2019 / Revised March 2, 2019 / Accepted March 22, 2019

Abstract: The polymer blend (PB) films consisted of poly(vinylidene fluoride) (PVDF) and poly(ethylene oxide) (PEO) with different compositional ratios (*i.e.*, PVDF/PEO =100/0, 75/25, 50/50, 25/75, and 0/100 wt%) have been prepared by solution casting method. These PB films were characterized by scanning electron microscopy (SEM), energy dispersive X-ray (EDX) spectroscopy, X-ray diffraction (XRD), Fourier transform infrared (FTIR) spectroscopy, and dielectric relaxation spectroscopy (DRS). The pristine films of PVDF and PEO have spherulite morphologies, which change enormously with the variation of their compositions in blend films. The EDX spectra confirm the linear variation of the amount of respective polymer elements, with the change of its compositional ratio in the PB films. The XRD and FTIR results confirm that the semicrystalline PVDF film has predominantly α- and β-phase crystals. The degree of crystallinity of these PB films exhibits non-linear increase, with increasing amount of PEO in the films. The relative fraction of the β-phase crystal of the PVDF in these complex PB films has been determined from the fractional relations based on the areas and intensities of crystalline peaks, observed in their XRD patterns which is found the maximum (~50%) for the 75 PVDF/25 PEO blend film. The dielectric dispersion of these PB films in the frequency window of 20 Hz-1 MHz at 27 °C reveals that the real part of the complex permittivity is governed predominantly by the interfacial polarization effect at lower audio frequencies, whereas it mainly depends on the polymer compositional ratio at higher radio frequencies. The segmental relaxation process peak of the PEO chain observed in the loss part of the electric modulus spectra, shifts toward the lower frequency side with a significant suppression of intensity as the amount of PVDF enhances in the PB films. This result confirms that the PEO dynamics face considerable hindrance by the PVDF structures. The dc electrical conductivity of these PB films increases non-linearly with increasing amount of PEO in the films, and varies by more than an order of magnitude with the variation of the compositional ratio over the entire range. The temperature-dependent study of 50 PVDF/50 PEO blend film confirms its thermally activated dielectric properties and the structural dynamics with the relaxation activation energy of 0.23 eV. The compositional ratio-dependent dielectric properties of PVDF/PEO blend films offer a promising potential for their use as dielectric permittivity- and electrical conductivity-tunable insulating materials, with engineered functionality for flexible electronics and electrical devices.

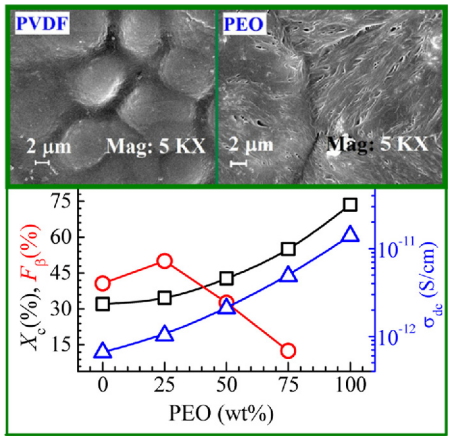

Keywords: PVDF/PEO blend, PVDF β-phase, degree of crystallinity, dielectric properties, electrical conductivity.

1. Introduction

In the last one decade, pristine poly(vinylidene fluoride) (PVDF; $[-CF_2-CH_2-]_n$) film and its matrix based polymer nanocomposite (PNC) films prepared by different methods have been extensively studied in order to examine and explore their promising properties. These films have diverse applications in the flexible electronics and electrical engineering devices, especially in the design and development of electroactive sensors and the high energy storage/harvesting devices.[1-15] The PVDF film exhibits outstanding physicochemical properties (viz. high resistance to chemical and thermal environment, weathering, and ultraviolet radiations),[2,4,14-17] relatively high dielectric constant and very low dielectric loss over the broad frequency range.[4-7,10,12-14] Further, the promising electroactive properties (piezo-, pyro- and ferroelectric) of its PNCs[2-6,11,17-20] have lead to the wide-range technological applications of these advanced multifunctional materials.[3,4,9-11,18,21-25] Most of the useful properties of the semicrystalline PVDF and its matrix based PNCs are associated with the relative fractions of the PVDF polymorphs crystal phases (α, β, γ, and δ). These

Acknowledgments: One of the authors (RJS) is grateful to the Department of Science and Technology (DST), New Delhi, for providing financial assistance for the experimental facilities through research projects Nos. SR/S2/CMP-09/2002, the DST-FIST program project No. SR/FST/PSI-134/2008, and also to the UGC, New Delhi, through SAP DRS-II program No. F.530/12/DRS-II/2016 (SAP-I). The author (PD) appreciatively acknowledges the award of Postdoctoral Fellowship (Research Associate) from the Council of Scientific and Industrial Research (CSIR), New Delhi. Authors also appreciate Prof. Beer Pal Singh, Department of Physics, CCS University, Meerut, India for extending the SEM facility.

***Corresponding Author:** Ram Jeewan Sengwa (rjsengwa@rediffmail.com, rjs.ph@jnvu.edu.in)

crystal phases mainly evolved during the preparation and/or subsequent modifications by various treatments of these materials.[2,4] The most relevant crystal structures of the PVDF from the technological point of view are the α- and β-phases. The α-phase of PVDF is non-polar, highly stable, and has 'trans-gauche-trans-gauche' (TGTG') chain conformation which is also similar for the δ-phase, whereas the β-phase is polar and relatively less stable having 'trans-trans-trans-trans' (TTTT) conformation, and further the γ-phase has T_3GT_3G' chain conformation.[1,2,4,16] Various experimental results have established that the high dielectric permittivity, and the piezo-, pyro-, and ferroelectric properties of the PVDF are predominantly associated with its β-phase crystal structure.[2,4,6,7,12-14] Therefore, it is technologically required to enhance the fraction of β-phase of the PVDF by transformation of its α-phase *via* various physical processing treatments or by the incorporation of different nanofillers (inorganic or organic) during the process of its matrix-based composite film preparation.[4,6,7,14,16,18,24,26,27]

Numerous studies have confirmed that the physicochemical properties and crystal phases of a PVDF film can be modified by blending it with other non-polar or polar polymers, and also simultaneous loading of the organic and/or inorganic nanofillers in the polymer blend matrix for the enhancement of their technological uses.[28-34] Among the polar polymers, poly(ethylene oxide) (PEO; $[-CH_2-CH_2-O-]_n$) is one of the most suitable hydrophilic matrices frequently used for the preparation of highly flexible-type solid polymer electrolyte (SPE) materials.[35-37] But the PEO based SPEs have poor thermal and mechanical properties due to the low melting temperature of the PEO matrix (~65 °C).[36,37] In contrast to PEO, the hydrophobic PVDF matrix is highly stable against thermal and mechanical deformation, and therefore, it is also considered as a promising material as a host matrix for the preparation of SPEs.[38,39] In the past few years, the blend of PVDF with PEO had been frequently used as a host matrix for the preparation of novel SPEs with a strategy to improve the thermal, mechanical, and electrochemical properties, and also enhancing their ionic conductivity for the design and development of safer and high performance ion conducting devices for energy storage/conversion.[40-49] In the preparation of these electrolytes, several researchers preferred the PEO-rich PVDF/PEO blend as host matrix because of the better compatibility and miscibility between the PVDF and PEO in such blends,[40-42,45,49] but some researchers used the PVDF-rich PVDF/PEO blend matrices.[47,48] The effects of the entire range of the blend compositional ratios on the properties of these blend based SPEs have also been studied by some others.[43] In these SPEs, a large cross-linkage of PEO and PVDF chains occurs through ion-dipolar coordination which results in high degree of homogeneity and relatively good miscibility of these hydrophobic and hydrophilic polymers in their solid and gel ion-dipolar complexes.[40-42,46-48] But, numerous studies on the pristine PVDF/PEO blend films have concluded that these films are either partially miscible in the PVDF-rich blends or have poor miscibility in the PEO-rich blends which further greatly changes with the variation in the compositional ratio of these polymers in their blends.[50-53]

In regards to the behaviour of various polymer blends, previous studies have revealed that the structural properties of a blend matrix are greatly affected by the individual polymer structural parameters (i.e., crystallinity, chain flexibility, polarity, polar group interaction ability, strength of hydrophilic and hydrophobic character etc.), the method adopted for the blend preparation, and also the possible electrostatic interaction of the inorganic or organic nanofillers with the blend matrix in their PNCs.[28-34,47,54-57] The recent work on the PVDF/PEO blends confirmed that the PVDF matrix acts as a confinement geometry for the PEO chains.[52,53] It was also concluded that the crystallization kinetics and phase morphology of the PEO structures confined between the PVDF crystals are highly dependent on the amount of PEO blended with PVDF and the procedure followed during the film formation from the blend solution.[53] Therefore, understanding the morphological, structural, dielectric, and electrical properties of different compositional ratios PVDF/PEO blend films and their chain segmental dynamics is of great importance for the realization of these PB films promising applications to be used as base matrices in the development of various technological advanced functional materials, especially for the next-generation energy storing devices and electroactive sensors.

Considering the above mentioned facts related to the potential applications of PVDF and PVDF/PEO blend matrices, in this paper, an attempt has been made to explore the effects of polymers compositional ratio on the morphology, polymorphic crystallite phases, degree of crystallinity, complex dielectric permittivity, electrical conductivity, and the PEO chain segmental dynamics of the solution cast PVDF/PEO blend films. Survey of literature reveals that all these properties of the PVDF/PEO blend films over the entire compositional range have not been systematically studied yet to the best of our knowledge, which are now first time addressed in-depth in the present manuscript. The fundamental aspects of various dielectric polarization processes involved in the dielectric dispersion and their correlation with the structural properties over the whole composition of the blends are the main focus of the present study.

2. Experimental

2.1. Materials

PVDF fine powder (M_w~534 kg mol^{-1}) and PEO granular powder (M_w=600 kg mol^{-1}) were acquired from Sigma-Aldrich, USA. The PVDF/PEO blend films of compositional ratios 100/0, 75/25, 50/50, and 25/75 wt% were prepared by dissolving these polymers in N,N-dimethyl formamide (DMF; spectroscopy grade, Loba Chemie, India) as a common solvent and then following the exact steps of solvent drying in the solution casting method as demonstrated earlier.[53] Initially, the required amounts of these polymers were dissolved together for each blend compositional ratio in the DMF by heating at 80 °C in stoppered conical glass flasks under continuous magnetic stirring until clear homogeneous polymeric solutions were attained. After that, these solutions were casted on to glass petri dishes and the solvent was allowed to evaporate at 70 °C on the microprocessor temperature controlled hot plate. Finally by cooling down the solvent evaporated materials to room temperature, the free-standing PVDF/PEO blend films were obtained. In this solution cast film preparation process, the PVDF crystallizes from the solu-

tion, whereas PEO crystallizes from the melt confined between the PVDF crystals because of the drying of the solution at 70 °C which is above the melting temperature (~65 °C) of the PEO. The pristine PEO film (*i.e.*, PVDF/PEO=0/100 wt%) was prepared by dissolving required amount of PEO in acetonitrile (ACN; Gradient Grade, Loba Chemie, India) and then following the simple solution casting method of solvent drying at room temperature. The thicknesses of the PVDF/PEO blend films of compositional ratios 100/0, 75/25, 50/50, 25/75, and 0/100 wt% are 0.20, 0.18, 0.18, 0.25, and 0.30 mm, respectively. All the films were further vacuum dried at 45 °C for 24 h in order to remove the solvent traces if any.

2.2. Measurements

The surface morphology and the elemental compositional study of the gold sputtered PVDF/PEO blend films were carried out by using the scanning electron microscope (SEM; Carl ZEISS EVO MA15) equipped with energy dispersive X-ray (EDX) analyzer. The X-ray diffraction spectra of the blend films were recorded in reflection mode of Cu-Kα radiation over the angular range 2θ from 10° to 40° by using a PANalytical X'pert Pro MPD diffractometer for the examination of crystalline phases and degree of crystallinity of these materials. The Fourier transform infrared (FT-IR) spectrometer (Agilent Technologies FT-IR spectrometer; Cary 630) was used in attenuated total reflectance (ATR) mode for recording the FT-IR spectra of the blend films over the wavenumber extending from 400 to 4000 cm^{-1}. Agilent technologies 4284A precision LCR meter equipped with 16451B solid dielectric test fixture of circular electrodes (38 mm diameter active electrode) was used for the dielectric and electrical measurements of the PB films by performing the dielectric relaxation spectroscopy (DRS) over the frequency window of six orders range (i.e., 2×10^{1} to 1×10^{6} Hz), at 27 °C. The temperature variation DRS study for the equal weight amount PVDF/PEO blend film was also performed. The details of the determination of various dielectric and electrical spectra of these films were the same as reported elsewhere.[57]

3. Results and discussion

3.1. Physical properties of the films

Figure 1 shows the digital photographs of different compositional ratio PVDF/PEO blend films. From these pictures, one can see that the pure PVDF film has relatively high optical transparency, whereas it greatly reduces with the increase of PEO concentration in the blends. The 75 PVDF/25 PEO and 50 PVDF/50 PEO blend films are brownish, and the 25 PVDF/75 PEO film is light brown, whereas the pure PEO film is milky white. Further, by the physical bending, it was noted that the PVDF film is relatively more rigid and less flexible, whereas the flexibility of the PVDF/PEO blend films enhances as the amount of PEO increases in the blends.

3.2. SEM and EDX spectra

The microstructures of the solution casted PB films including

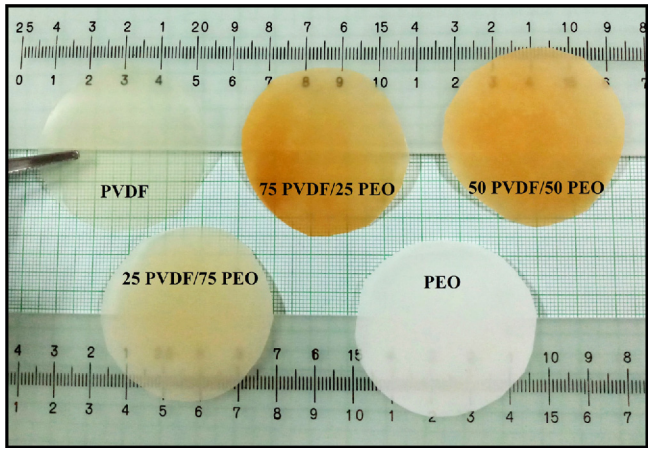

Figure 1. Digital photographs of the pristine PVDF film, PVDF/PEO blend films, and the pristine PEO film.

pure PVDF, pure PEO, and the different compositional ratio PVDF/PEO are examined from their SEM images depicted in Figure 2(a)-(e). It can be noted from Figure 2(a) that the top surface of the PVDF film (*i.e.*, the solvent evaporated surface of the film in the petri dish) has different microsizes grain-like spherulites (some are encircled) which are attributed to its α-phase crystals. Some oriented fibril-like small textures between the spherulites can also be noted (some structures are distinguished by rectangular boundaries) which represent the β-phase crystals. These characteristic morphological features of the solution casted PVDF film had also been observed by the earlier investigators.[9,14,58,59] Further, the grain-like features confirm that the α-phase spherulites of the PVDF contain acicular crystallites emanating in a radial direction from the centre.[59] Figure 2(e) shows that the solvent evaporated surface of the pristine PEO film has relatively bigger size spherulites with microcracks and pores confirming its semicrystalline structure quite in agreement with that demonstrated earlier.[42,43] The formation of microcracks and pores at the PEO surface are expected owing to the fast evaporation of the solvent (ACN) during the film casting process.

Figure 2(b)-(d) shows the entirely different and highly complex surface morphology of the PVDF/PEO blend films as compared to that of the microstructures of pristine PVDF and pristine PEO films. As seen in Figure 2(b), the surface of 75 PVDF/25 PEO blend film is relatively smooth with several irregular shape clusters regarding the nature of PVDF and PEO crystals. This may be owing to the disappearance of bigger size pristine polymers spherulites leaving only local inhomogeneity in the blend film.[43,52,55] The 50 PVDF/50 PEO blend film morphology (Figure 2(c)) confirms that there are rough spherulites and small size pores, with a large homogeneity of the structures with highly symmetrical morphology which fairly matches with the results of nearly same compositional ratio blended PVDF/PEO films.[47,52] Figure 2(d) shows that the surface of 25 PVDF/75 PEO blend film has different sizes PEO aggregates which represent the excess amount of PEO that remains immiscible. In this blend film, these types of PEO aggregates are expected probably due to the high concentration of PEO that has not become competent with the PVDF. During the process of film preparation, the cooling of

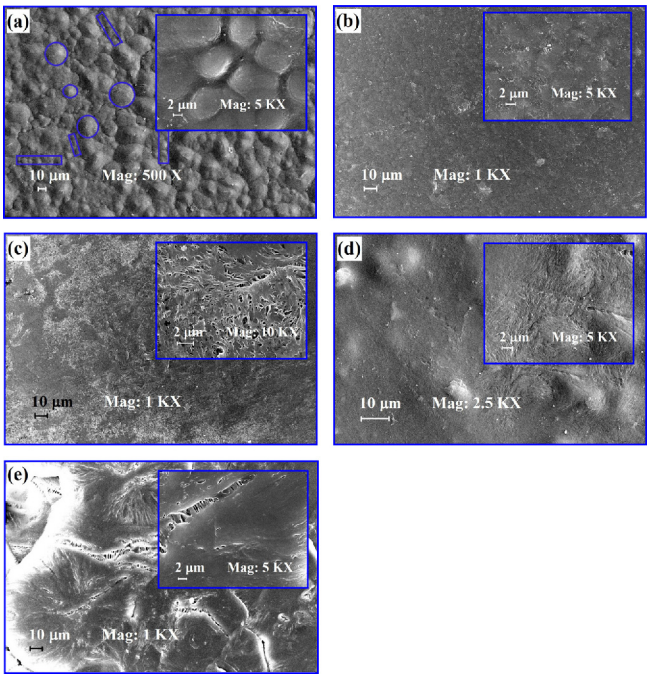

Figure 2. SEM images of (a) the pristine PVDF film, (b-d) PVDF/PEO blend films (b; 75/25, c; 50/50, d; 25/75 wt%), and (e) the pristine PEO film at different scales and magnifications. Insets show the micrographs at 2 μm with increased magnifications.

blend material to the room temperature after the solvent (DMF) evaporation at 70 °C, the molten PEO recrystallizes and agglomerates which may result in such type of morphology of the PEO-rich PVDF/PEO blend film.[41]

The EDX mapping of the PVDF/PEO blend films was performed in regards to the analysis of sample purity and the blended amounts of the polymers based on the presence of various elements in the polymer matrix and their weight% and atomic% with the change in the compositional ratio of the blend films.[24,55,57] The EDX spectra of the PVDF/PEO blend films are shown in Figure 3(a)-(e) where the Y-axis has the counts (number of X-rays received and processed by the detector) corresponding to the various elements present in the films and the X-axis shows the energy level of those counts. The analytical compositions (weight% and atomic%) of the blend films obtained from the EDX spectra are given in Table 1. The EDX spectrum of pristine PVDF film (Figure 3(a)) shows strong peaks of the carbon (C) (at 0.28 keV) and fluorine (F) (at 0.68 keV) elements as expected in this film from its chemical formula, without any other impurity peaks. Similarly, the pristine PEO film has the C and oxygen (O) elements according to its chemical formula and there is no signature of other elements in its EDX spectra (Figure 3(e)). The characteristic X-ray energy peak corresponding to the O element is observed at 0.53 keV for the PEO film. All the PVDF/PEO blend films exhibit only the energy peaks of C, F, and O elements (Figure 3(b)-(d)), which also evidence the purity of these polymer blend films. The additional peaks observed around 1.63 and/or 2.15 keV (Figure 3(a)-(e)) are of gold (Au) element which have appeared due to the gold sputtering which was done over the sample surface for the EDX mapping.

The obtained amounts of the C, F, and O elements (i.e., weight

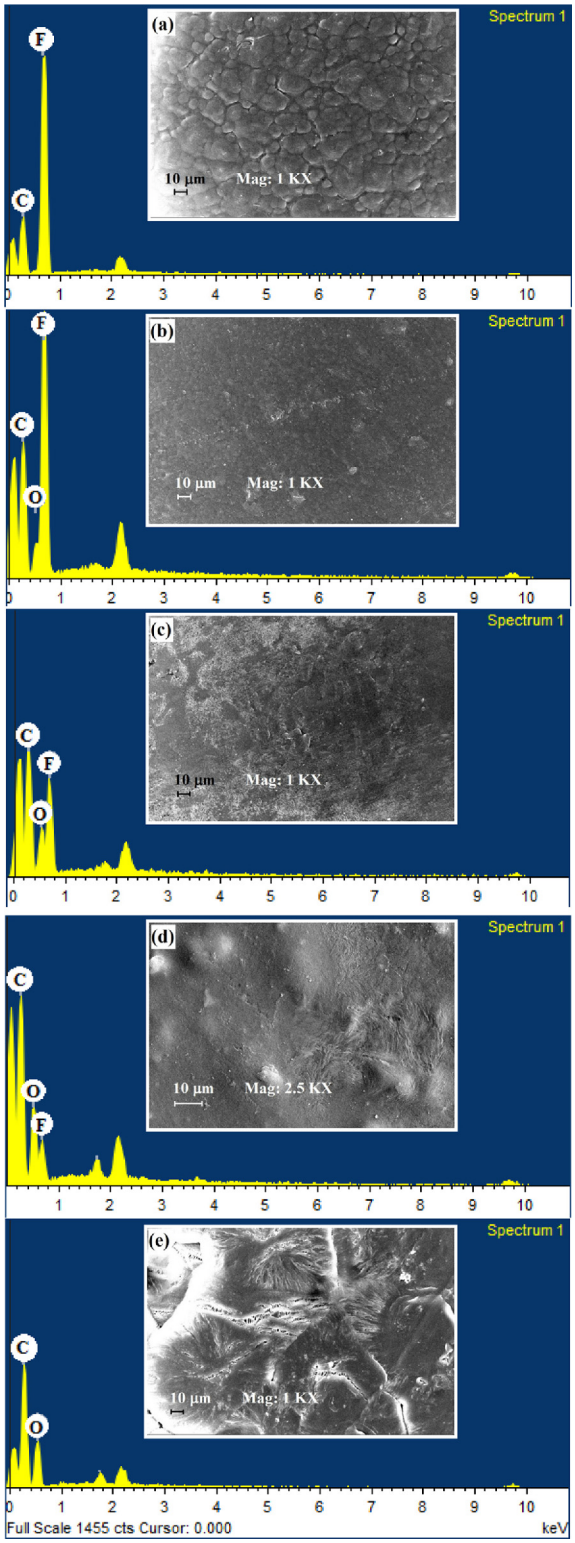

Figure 3. The EDX spectra of (a) the pristine PVDF film, (b-d) PVDF/PEO blend films (b; 75/25, c; 50/50, d; 25/75 wt%), and (e) the pristine PEO film.

percentage (wt%) and atomic percentage (At%)) of the PVDF/PEO blend films are given in Table 1. The elemental amount of pure PVDF (Table 1) is found in agreement of the literature.[24] As seen from Table 1, the wt% of the F element decreases, whereas the O element increases with the increase of PEO amount in the blend films, which is expected according to the composition

Table 1. The electron energy shells corresponding to X-ray emission for C, F, and O elements, their weight percentages (wt%), and the atomic percentages (At%) in the PVDF film, PVDF/PEO blend films, and the PEO film obtained from the EDX spectra

Element	X-ray shell	wt%	At%
Pure PVDF film			
C	K	33.99	44.88
F	K	66.01	55.12
Total		100.00	100.00
75 PVDF/25 PEO blend film			
C	K	36.20	46.68
F	K	55.28	45.07
O	K	8.52	8.25
Total		100.00	100.00
50 PVDF/50 PEO blend film			
C	K	41.56	51.46
F	K	39.35	30.80
O	K	19.09	17.74
Total		100.00	100.00
25 PVDF/75 PEO blend film			
C	K	50.21	58.69
F	K	20.66	15.45
O	K	29.13	25.86
Total		100.00	100.00
Pure PEO film			
C	K	58.53	65.00
O	K	41.47	35.00
Total		100.00	100.00

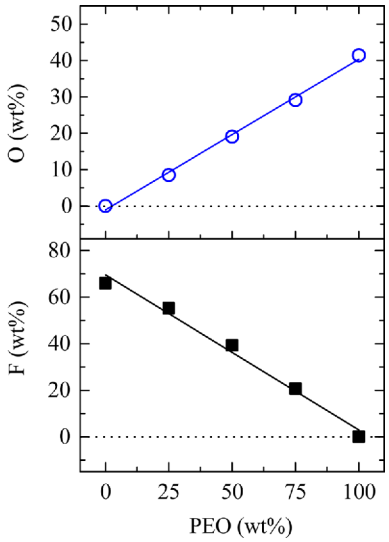

Figure 4. The plots of the F and O elements (wt%) versus PEO (wt%) in different compositional ratios PVDF/PEO blend films.

weight ratios of the PVDF and PEO in the blends. Figure 4 depicts the plots of the F and O wt% versus PEO (wt%) in the PVDF/PEO blend films. These plots are quite linear over the entire range of PEO concentration in the blend films. This finding confirms that the amounts of PVDF and PEO have uniform distribution in their blend matrices.

3.3. XRD spectra

The XRD spectra of pristine PVDF film, PVDF/PEO blend films, and the pristine PEO film, as a function of the scattering angle 2θ, are presented in Figure 5. All these films exhibit some intense and sharp peaks, and also several weak diffraction peaks confirming their semicrystalline structures. The values of angular positions (2θ), intensities (I), and full width at half maximum (FWHM) for the major crystalline peaks of these PB films were evaluated using X'pert pro® software. The obtained values of these parameters are listed in Table 2 along with the (hkl) indices corresponding to the reflection planes of the PVDF and PEO crystals. The values of crystal structure parameters namely, basal-spacing (d) and crystallite size (L) for these films (Table 2) were determined using the Bragg's Eq. (1) and the Scherrer Eq. (2), respectively;

$$d = \lambda/2\sin\theta \quad (1)$$

$$L = 0.94\lambda/\beta\cos\theta \quad (2)$$

The enlarged view shown in the lower layer of Figure 5(a) confirms that the diffractogram of pristine PVDF film has major intense diffraction peaks at 2θ=18.82°, 20.53°, and 27.13°. In addition to these intense peaks, some weak diffraction peaks at 2θ=33.63°, 36.62°, 38.29°, and 39.08° are also noticed in the XRD spectrum of pristine PVDF film. Survey of literature verifies that the PVDF film prepared by any of the film preparation methods was firstly characterized by the XRD measurements in order to confirm the nature of crystal phases formed in the film and to identify its suitability as a base matrix in the preparation of electroactive polymer nanocomposites.[1-5] The characterization of the fraction of crystal phases is technically needed because most of the applications of PVDF film itself and also of the composite materials based on its matrix depend on the existence of a particular type of crystal phase in the films.[2-4] In the recent review on the electroactive crystal phases of PVDF,[2] it was summarized that the major diffraction peaks exhibited at 2θ=17.66°, 18.30°, 19.90°, and 26.56° are corresponding to the α-phase crystal of reflection planes (100), (020), (110), and (021) respectively. Further, the peak of its β-phase crystal of reflection planes (110), (200) has mostly been assigned to 20.26°. The γ-phase crystal peaks of PVDF are commonly exhibited at 18.5° (020), 19.2° (002), and 20.04° (110). But in the same review,[2] it was also concluded that the XRD results of various researchers have lead to some confusion between the assignments of α- and β-phase crystals of the PVDF film. Further, some recent studies have undoubtedly assigned the peaks of 2θ values 20.6°,[6,18,27] 20.5°,[60] 20.45°,[22] 20.4°[61] to the β-phase crystal of the PVDF instead of its most accepted 2θ value 20.26°,[2] which may be because of a small difference in these peak positions.

In the present study, according to the literature, the intense diffraction peak observed in the XRD pattern of PVDF (lower layer of Figure 5(a)) at 2θ=20.53° (110), (200) is assigned to the β-phase crystal,[6,18,22,27,60] whereas the another intense peak at 2θ=18.82° (020) is attributed to the α-phase crystal.[22,61] Further, the relatively less intense peak appeared at 2θ=27.13° (022) also represents the α-phase crystal of the PVDF film which is in

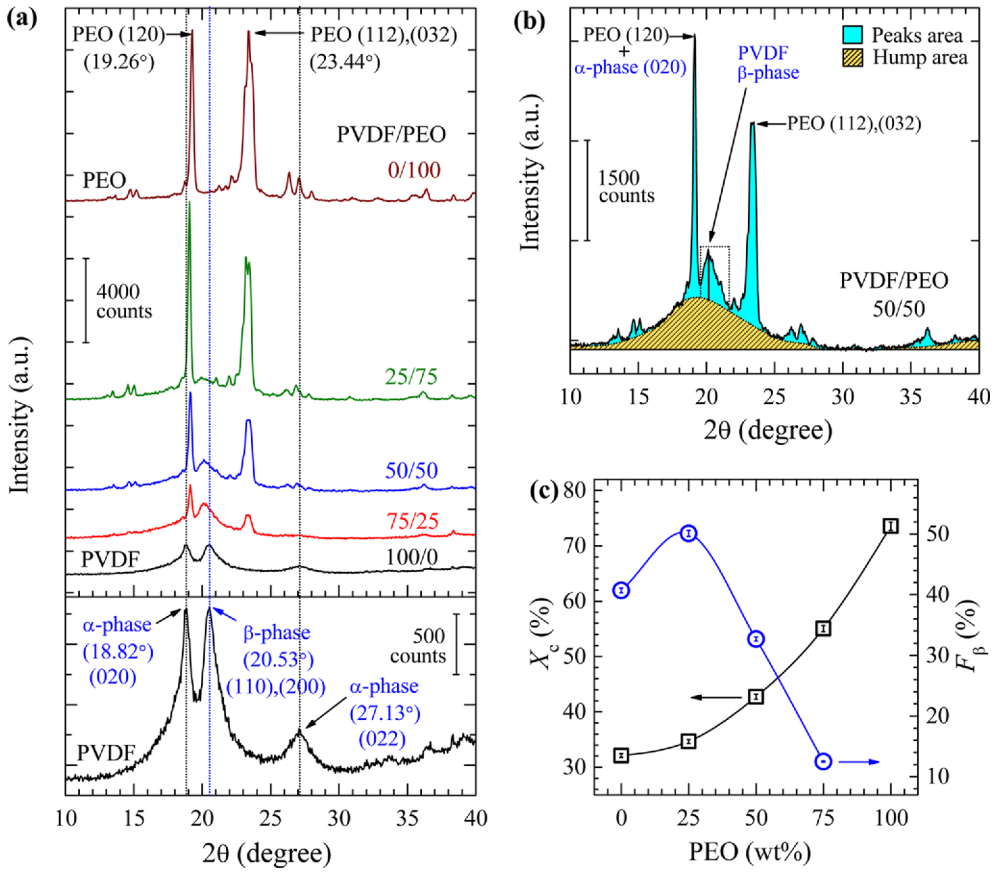

Figure 5. (a) The XRD patterns of different compositional ratios PVDF/PEO blend films. The enlarged view of pristine PVDF film is shown in the lower layer labeled with its crystallite phases. (b) The XRD pattern of the 50 PVDF/50 PEO blend flim highlighting the areas with the crystalline peaks and hump. (c) The plots of the degree of crystallinity (X_c) and the relative fraction of the β-phase crystal (F_β) of PVDF versus PEO (wt%) concentration of the PVDF/PEO blend films. Error bars for X_c and F_β are marked in the plots.

agreement with the earlier study.[22] These XRD results confirm that the prepared PVDF film is polymorphs of α- and β-phases. Further, from the XRD pattern of the PVDF, it can be noted that the peaks intensities of 18.82° and 20.53° are nearly equal, whereas the 27.13° peak intensity is about one-third than that of the intense peaks of the film. Figure 5(a) shows that the pristine PEO film scattering pattern has highly intense characteristic diffraction peaks at 19.26° (120) and 23.44° (112), (032) which confirm its high degree of crystallinity, and this XRD pattern is in good agreement with the results reported elsewhere.[62,63]

The alteration in α- and β-phases of the PVDF crystallites due to its blending with the PEO at different compositional ratios can be examined by noting the relative changes in these polymers characteristic peaks positions and their intensities given in Table 2. From Figure 5(a), it is observed that the α-phase crystal peak (18.82°) of the PVDF is overlapped by the intense crystalline peak (19.26°) of PEO which results in a new peak between these two characteristic peaks, and there is a slight shift of the β-phase crystal peak (20.53°) to the lower angle with anomalous variation in its intensity as the PEO concentration increases in the blend films. Further, the intensity of PEO peaks greatly enhances with the increase of its content in the PVDF/PEO blend films which is as expected because of the relatively very high peaks intensities of the pristine PEO (Table 2). It has also been noted that the α-phase crystal peak (27.13°) of the PVDF is suppressed in all these compositional ratios PVDF/PEO blend films. From Table 2, it can be further noted that the pristine PVDF peak of β-phase (20.53°) has appeared at 20.20° and 20.17° for the 75 PVDF/25 PEO and 50 PVDF/50 PEO blend films, respectively, which is in good agreement with the most acceptable value of β-phase crystal peak position of the PVDF (*i.e.*, 20.26°) as summarized in the review.[2] But for 25 PVDF/75 PEO blend films, it is very weak and found at 19.95° which infers the coexistence of small fraction γ-phase crystal (20.04°)[2] with that of the β-phase crystal of the PVDF.[2,19,47] These structural properties infer that there is a partial phase transformation and alteration of the PVDF crystals on its blending with PEO which is largely influenced by the compositional ratio of the polymers in these PB films. From Table 2, it can be noted that there is a variation in the *d*, *L*, and *I* values of the various crystal reflection planes with the increase of PEO concentration in the blends which also infers existence of some kind of specific molecular interactions mainly between the >CF_2 groups of PVDF and the C-O-C units of PEO chains.

The percentage degree of crystallinity X_c (%) of these polymers and their blend films was determined using the total area of crystalline peaks A_P and hump area A_H from the relation (3);[48,64-66]

$$X_c\,(\%) = A_p/(A_P+A_H) \times 100 \qquad (3)$$

The A_P and A_H portions of the 50 PVDF/50 PEO blend film as a representative are highlighted in its XRD pattern shown in Fig-

Table 2. Crystal reflection plane indices (*hkl*), Bragg's angle 2θ, basal spacing *d*, full width at half maximum FWHM, crystallite size *L*, and peak intensity *I* of the diffraction peaks of the PVDF film, PVDF/PEO blend films, and the PEO film

hkl	2θ (deg)	*d* (nm)	FWHM ($\times 10^{-3}$ rad)	*L* (nm)	*I* (counts)	Comments
Pure PVDF film						
(020)	18.82	0.4713	10.63	13.81	870	α-phase
(110), (200)	20.53	0.4322	15.38	9.57	890	β-phase
(022)	27.13	0.3285	26.53	5.62	310	α-phase
75 PVDF/25 PEO blend film						
PVDF (020) + PEO (120)	19.14	0.4635	4.64	31.63	1907	PVDF and PEO peaks coalesce
PVDF (110), (200)	20.20	0.4392	18.38	8.00	1033	peak shifts towards lower angle
PEO (112), (032)	23.35	0.3806	9.56	15.46	811	peak shifts towards lower angle
50 PVDF/50 PEO blend film						
PVDF (020) + PEO (120)	19.14	0.4635	4.40	33.39	3936	PVDF and PEO peaks coalesce
PVDF (110), (200)	20.17	0.4399	16.30	9.02	723	peak shifts towards lower angle
PEO (112), (032)	23.39	0.3800	9.98	14.81	3014	peak shifts towards lower angle
25 PVDF/75 PEO blend film						
PVDF (020) + PEO (120)	19.07	0.4651	3.87	37.90	8800	PVDF and PEO peaks coalesce
PVDF (110), (200)	19.95	0.4448	12.95	11.35	287	peak shifts towards lower angle
PEO (112), (032)	23.34	0.3808	10.23	14.46	6420	peak shifts towards lower angle
Pure PEO film						
(120)	19.26	0.4604	4.56	32.24	7838	crystalline phase
(112), (032)	23.44	0.3792	12.99	11.39	7835	crystalline phase

ure 5(b). The A_P and A_H portions are separated by drawing the best arbitrary chosen line (dotted) between the XRD pattern and the baseline using the OriginPro® version-8 software from which the values of these areas are determined. The evaluated X_c values for these PVDF/PEO blend films are given in Table 3 and also graphically represented in Figure 5(c). The X_c versus PEO (wt%) plot confirms that the degree of crystallinity of these PB films non-linearly increases with the increase of PEO amount in the films.

In general, the relative fractions of various crystal phases present in a PVDF film and its based PNC films are determined by noting the absorption bands intensities of these phases from their FTIR spectra and substituting these values in the Lambert-Beer's law with the assumption that the FTIR absorption of these materials follows this law.[2,17,18,19,26,27,67] In case of PVDF/PEO blend films, this law cannot be applied because of the fact that the PEO has an intense absorption band of its C-O stretching vibrational mode at 840 cm^{-1},[64,68-71] and at the same wavenumber the PVDF exhibits its main characteristic β/γ phase absorption band due to the CF_2 stretching.[2,19,67] We noticed that there are numerous studies on the PVDF/PEO blends and these blend matrices based SPE materials,[40-53] but the estimations of the relative fractions of the crystal phases of PVDF were not attempted even though the researchers have measured the FTIR and/or XRD spectra of the materials in these studies except one.[52] In this study, the authors determined the relative fraction of β-phase in the PVDF/PEO blend films but they did not consider the above mentioned fact regarding overlapping of the 840 cm^{-1} vibrational band of both the polymers. For such type of complex systems, here we propose two simple relations for estimation of the relative fraction of β-phase (F_β) crystals of PVDF and its transformation (*i.e.*, relative changes) in the PVDF/PEO blend films with respect to that of the pristine PVDF film when the films are prepared by the same method under identical conditions. These relations are based on the areas of crystal phases peaks and their intensities in the XRD patterns of the PVDF/PEO blend films as given in the following Eqs. (4) and (5), respectively;

$$F_\beta(\%) = A_{C(\beta)}/A_{C(T)} \times 100 \quad (4)$$

$$F_\beta(\%) = I_\beta/I_T \times 100 \quad (5)$$

where in Eq. (4), $A_{C(\beta)}$ is the area of β-phase crystal peak in the XRD pattern of PVDF/PEO blend film and $A_{C(T)}$ is the total area of all the crystal phases peaks of the pristine PVDF film (*i.e.*, $A_{C(\alpha)}$ (18.82°)+$A_{C(\beta)}$ (20.53°)+$A_{C(\alpha)}$ (27.13°)). Similarly, in Eq. (5), I_β is the intensity of β-phase crystal peak of the PVDF/PEO blend film and I_T is the total intensity of the peaks of pristine PVDF film (*i.e.*, I_α (18.82°)+I_β (20.53°)+I_α (27.13°)). Recently, the F_β (%) values were also determined using *I* values from the XRD patterns of the PVDF matrix based electroactive nanocomposites.[6,72] In the present study, the *I* values of the PVDF crystal phases peaks observed in its XRD pattern are taken equal to the peak height from the dotted line (*i.e.*, the line separating the amorphous part (hump) and the crystalline part) to the top of the peak as marked for the β-phase in Figure 5(b). The *I* values noted from the XRD patterns for the crystal phases of PVDF/PEO blend films are listed in Table 2.

The estimated values of F_β from Eqs. (4) and (5) for the PVDF/PEO blend films are recorded in Table 3. One can see from Table 3 that the F_β values obtained from the peaks areas and the peaks intensities are nearly the same which also confirm the validity of their relations given in Eqs. (4) and (5) for the correct estimation of F_β. Further, the average values of these F_β (%) values

Table 3. The values of degree of crystallinity X_c (%), and the relative fraction of β-phase F_β (%) calculated from the β-phase crystal peaks areas (Eq. (4)), intensities (Eq. (5)) of the diffraction peaks in the XRD patterns, and the amount of β-phase crystal transformation ΔF_β (%) = $F_{\beta(blend)}$ (%) - $F_{\beta(PVDF)}$ (%) of the PVDF/PEO blend films

Polymer films	X_c (%)	F_β (%)		F_β (%) (Avg.)	ΔF_β (%) (Avg.)
		From Eq. (4)	From Eq. (5)		
Pure PVDF	32.1	38.4	43.0	40.7	-
75 PVDF/25 PEO	34.7	50.3	49.9	50.1	9.4
50 PVDF/50 PEO	42.7	30.5	34.9	32.7	-8.0
25 PVDF/75 PEO	55.1	11.2	13.8	12.5	-28.2
Pure PEO	73.6	-	-	-	-

of the PVDF/PEO blend films are determined and the same are also plotted in Figure 5(c). This shows that the PVDF-rich blend film has high F_β, whereas 50/50 wt% and PEO-rich blend films have low F_β in relation to that of the F_β value of the pristine PVDF film which directly provides the information about the amount of β-phase crystal changed in the PVDF/PEO blend films with the variation of the blend compositional ratio. The average value of the β-phase crystal alteration in the PVDF/PEO blend films is determined from the relation ΔF_β (%)=$F_{\beta(blend)}$ (%)-$F_{\beta(PVDF)}$ (%). The values of ΔF_β (%) given in Table 3 show that the addition of 25 wt% amount of PEO in the PVDF enhances the β-phase, whereas the 50 wt% blending of PEO with PVDF has a negative effect on the β-phase transformation. In the PEO-rich PVDF/PEO blend film (*i.e.*, for 75 wt% blending of PEO), the ΔF_β is highly negative which reveals that there is a huge destruction of the β-phase crystals at this composition of the blend film.

3.4. FT-IR spectra

Figure 6 depicts the FT-IR spectra of PVDF/PEO blend films over the wavenumber range extending from 400 to 4000 cm^{-1}. The wavenumbers segments from 1500 to 2750 cm^{-1} and 3200 to 4000 cm^{-1} are omitted from these spans, and also to get enlarged view of prominent characteristic peaks in the range 400-1500 cm^{-1}, so that the vibrational bands related to the presence of various crystal phases of the PVDF can be clearly identified. The wavenumbers of various characteristic IR absorption band

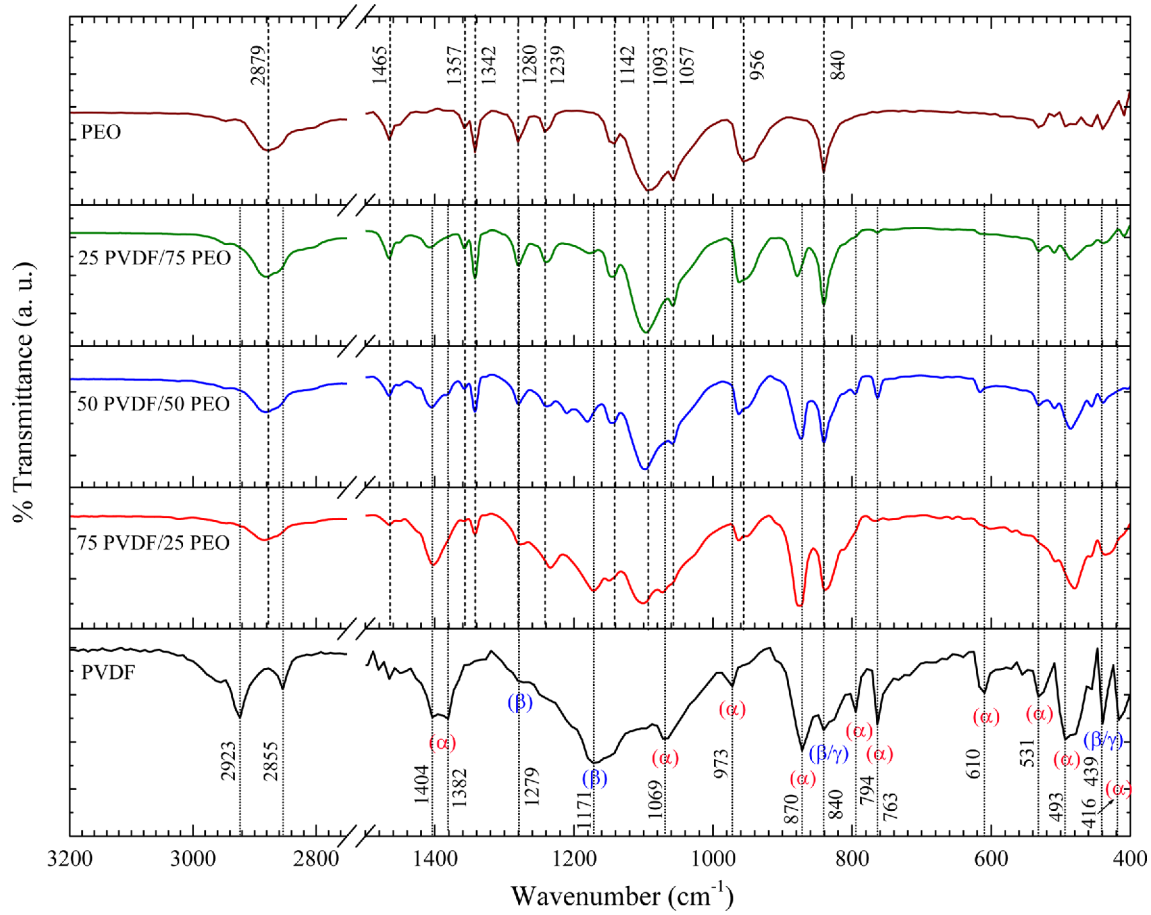

Figure 6. FTIR spectra of the pure PVDF film, PVDF/PEO blend films, and the pure PEO film. The wavenumbers of various vibrational bands are marked in the figure for pristine PVDF and PEO films.

peaks of the pristine PVDF and also the PEO are marked in their respective spectrum, and these values are also listed in Table 4 with the band assignments as reported in the literature for the PVDF[2,5,18,19,45,61,67] and PEO.[56,64,68-71] Further, the α, β-, and γ-phases bands of the PVDF noted in its spectrum are also marked in the figure for their exact location and the relative intensity comparison.

It can be read from the lower layer of Figure 6 that the pristine PVDF exhibits various characteristic vibrational bands at 416, 493, 531, 610, 763, 794, 973 cm^{-1}, and doublet at 1382-1404 cm^{-1} which attribute to its non-polar α-phase crystals.[2] The band exhibited at 439 cm^{-1} represents a combined effect of β- and γ-phase crystals, whereas a shoulder band at 840 cm^{-1} and very weak band at 1279 cm^{-1} belong to the β-phase crystal of the semicrystalline PVDF which are consistent with the assigned vibrational band of this polymer in the literature.[2,5,18,19,27,52,61,67,73-75] Further, the bands appearing at 870, 1069, 1171, and 2923 cm^{-1} are corresponding to the $>CF_2$ vibrational mode, CH_2 wagging mode, $>CF_2$ stretching mode, and CH_2 asymmetric stretching mode, respectively.[2,19,27,73-75] The PEO spectrum has peaks at 840, 956, a triplet centered at 1093 (1057, 1142), 1239, 1280, 1342 and 1465 cm^{-1} corresponding to C-O stretching, CH_2 asymmetric rocking, symmetric and asymmetric C-O-C stretching, CH_2 symmetric twisting, CH_2 asymmetric twisting, CH_2 bending, and C-H bending of CH_2, respectively as assigned earlier.[68-71]

The addition of PEO in the PVDF has lead to huge alteration in the characteristic vibrational modes of the PVDF which further changes with the variation of PVDF/PEO blend compositional ratio as can be noticed from Figure 6. The vanishing and shifting of characteristic bands and appearance of some new bands corresponding to the pristine PVDF and PEO bands in the PB films, and also the increase or decrease of intensities of some bands and their broadening have affirmed the significant interactions between the PEO and PVDF chain segments. In the review article,[2] it was concluded that the IR bands of wavenumbers 408, 532, 614, 766, 795, 855, and 976 cm^{-1} represent the α-phase crystal of PVDF, whereas the 510, 840, and 1279 cm^{-1}, and 431, 512, 776, 812, 833, 840, and 1234 cm^{-1} belong to the β-phase and γ-phase, respectively. It was also confirmed that the band at 445 cm^{-1} and the shoulder band at 1279 cm^{-1} are exclusively for the β-phase, although 840 cm^{-1} is common for both the β- and γ-phases, it is strong for just the β-phase, whereas it appears as a shoulder of 833 cm^{-1} band for the γ-phase alone. The FTIR bands at 439, 840, and 1171 cm^{-1}, as listed in Table 4, validate the existence of β-phase crystals in the PB films.

The FTIR spectrum of 75 PVDF/25 PEO blend film (Figure 6)

Table 4. Wavenumbers corresponding to different vibrational modes and their assignments to the functional groups of PVDF, PEO, and PVDF/PEO blend films

PVDF and PEO band assignment		Wavenumber (cm^{-1})					Comments
		Pure PVDF	75 PVDF/ 25 PEO	50 PVDF/ 50 PEO	25 PVDF/ 75 PEO	Pure PEO	
PVDF	α-phase	416 (α)	-	-	-	-	Vanished
PVDF	β- and γ-phases	439 (β/γ)	435	-	-	-	Red shift
PVDF	CF_2 bond wagging	493 (α)	478	485	484	-	Red shift
PVDF	CF_2 bond bending	531 (α)	-	-	-	-	Diminished
PVDF	CF_2 skeletal bending	610 (α)	-	619	-	-	Blue shift
PVDF	CF_2 skeletal bending	763 (α)	-	-	-	-	Diminished
PVDF	CH_2 rocking	794 (α)	-	-	-	-	Diminished
PVDF PEO	CH_2 rocking, CF_2 stretching, skeletal C-C stretching C-O stretching	840 (β/γ)	840	841	840	840	No change
PVDF	CH_2 stretching	870 (α)	874	871	879	-	Blue shift
PEO	C-O stretching vibration with CH_2 asymmetric rocking motion	-	960	962	960	956	Blue shift
PVDF	CH_2 rocking	973 (α)	-	-	-	-	Vanished
PVDF	CH_2 wagging	1069 (α)	1074				Blue shift
PEO triplet	C-O-C symmetric and asymmetric stretching (intense centre peak of amorphous phase and two shoulders of crystalline phase)	-	-	1058	1058	1057	Blue shift
		-	1102	1099	1096	1093	
		-	1149	1143	1143	1142	
PVDF	CF_2 symmetric stretching	1171 (β)	1174	1182	-	-	Blue shift
PEO	CH_2 symmetric twisting	-	1233	1239	1241	1239	Anomalous
PEO	CH_2 asymmetric twisting	-	-	1280	1280	1280	No change
PEO doublet	CH_2 bending and wagging (crystalline phase)	-	1342	1342	1342	1342	No change
		-	1357	1357	1357	1357	
PVDF	CF_2 symmetric stretching	1382, 1404 (α)	1403	1404	1407	-	Anomalous
PEO	C-H bending of CH_2	-	-	1463	1464	1465	Red shift
PVDF	CH_2 symmetric stretching	2855	-	-	-	-	Vanished
PEO	CH_2 asymmetric stretching	-	2882	2883	2880	2879	Anomalous
PVDF	CH_2 asymmetric stretching	2923	-	-	-	-	Vanished

reveals that the addition of PEO (25 wt%) in the PVDF intensifies the 840 cm^{-1} band with more distinguishable doublet and also vanishes several lower wavenumbers bands of the PVDF as mentioned in Table 4. Further, for the PEO its crystallite shoulder peak (1357 cm^{-1}) in the doublet is absent, and the shoulder peaks (1057 and 1142 cm^{-1}) of the triplet are weakened along with a huge broadening confirming a large alteration of the PEO crystallites in the PB film. As the PEO amount increases, the shoulder peaks of doublet and triplet enhance confirming the increase of PEO crystallites which is in agreement with the X_c (%) values of these blend films determined from their XRD patterns. In these blend films, the intensity of 840 cm^{-1} peak of PVDF crystal (β-phase) gradually enhances with the increase of PEO amount which is owing to its coalescing with the PEO band at the same wavenumber. Further, the PVDF doublet (2923 cm^{-1} and 2855 cm^{-1}) have also merged with the PEO peak at 2879 cm^{-1}.

In addition to above listed changes, Table 4 shows that the 416, 531, 763, and 794 cm^{-1} bands corresponding to the α-phase crystal of PVDF have highly diminished in all the blend films, whereas the vibrational band at 493 cm^{-1} has appeared at lower wavenumber (*i.e.*, in the range 478-486 cm^{-1}) in the blend films. Further, the 439 cm^{-1} band of PVDF is found at 435 cm^{-1} which is prominent in the 75 PVDF/25 PEO blend film, and the 610 cm^{-1} band of PVDF has appeared at 619 cm^{-1} which is only in the 50 PVDF/50 PEO blend film. The 840 cm^{-1} peak corresponding to the β-phase crystal of PVDF also shows a prominent increase in intensity with the increase of PEO concentration up to 75 wt% into the blend matrix. The alterations of some peaks positions between 1233-1280 cm^{-1} in the PVDF/PEO blend films indicate the presence of γ-phase but the contribution of the CH_2 symmetric and asymmetric twisting due to PEO interactions in these bands cannot be neglected for this change.[52] Besides the bands shifting, there are some variations in the intensities of 870, 1069, 1171 cm^{-1} bands, and also 1340, 1382-1404 and 2855-2883 cm^{-1} bands as compared to that of the pristine PVDF and the PEO, respectively, which confirm enormous alteration in the polymer-polymer interaction with the variation in compositional ratio of these PB films. Finally, it is concluded that upon addition of PEO in the PVDF and their concentration variation over the entire compositional ratio, some of the peaks have either weakened or disappeared, and some new peaks have appeared confirming the alteration in relative amounts of crystallite phases of the PVDF, which is in agreement with the earlier study on the PVDF/PEO blend films having the PVDF-rich composition.[61] Further, these structural results are consistent with the XRD results on the crystallinity and crystal phases of these PVDF/PEO blend films as discussed in detail above.

3.5. Dielectric spectra

Figure 7(a) shows the complex dielectric permittivity (real part ε' and imaginary part ε'') and $\tan\delta=\varepsilon''/\varepsilon'$ spectra of PVDF/PEO blend films over the frequency range from 20 Hz to 1 MHz, at 27 °C. The ε' value of pristine PVDF film is 4.19 at 20 Hz, and it decreases gradually with the increase of frequency and finally approaches 3.40 at 1 MHz. The frequency-dependent ε' values of the pristine PVDF film are found in good agreement with the earlier results.[75,76] So far, enormous work had been carried out on the frequency- and temperature-dependent dielectric dispersion of the PVDF films prepared by various methods, and their 10 Hz to 100 Hz frequency window ε' values were reported in the range from ~4 to 15, at ambient temperature which exhibit a little decrease against the increase of frequency.[6,7,13,27,32,60,61,75,77-84] In fact, the ε' of a PVDF film strongly depends on the type of crystal phases present therein and the relative fraction of these phases.[1-5] The α-phase is non-polar, whereas the β-phase is polar and therefore, the PVDF film having dominance of β-phase exhibits relatively higher ε' values.[5,32] In the present study, the F_β value is found ~0.41 for the PVDF film (Table 3) which is low as compared to the ~0.6 value of the F_α (*i.e.*, 1-F_β) for this bi-phase film, and therefore, the frequency-dependent ε' values of this PVDF film are found in the range 4.19 to 3.40 with change of frequency from 20 Hz to 1 MHz which are low and comparable to that of the α-phase crystal dominated PVDF film.[76] Further, From Figure 7, it can be noted that the frequency-dependent ε'' and $\tan\delta$ values of the PVDF film are low and exhibit the minimum around 15 kHz. The frequency-dependent $\tan\delta$ values and the shape of its spectrum for the PVDF film are found reasonably in good agreement with the earlier results.[13,27,75] Among the synthetic polymers, the PVDF film has relatively high ε' and very low $\tan\delta$ values and also bears high thermomechanical properties. Therefore owing to such type of properties, it offers a potential candidacy for the preparation of promising PNCs suitable in the design and fabrication of high quality capacitors for the electrical energy storage[5-7,13,14,77,85-87] with their workability over the broad frequency range.

The ε' values of the pristine PEO film are slightly higher than 2 in the high frequency range from 100 kHz to 1 MHz as can be noted from the inset of Figure 7, but these values non-linearly increase with the decrease of frequency in the audio frequency (AF) region which approaches 12.3 at 20 Hz. This type of dielectric dispersion behaviour of the semicrystalline PEO film is mainly due to enhancement of the interfacial polarization (IP) effect at the boundaries of its crystalline and amorphous domains which contributes in the bulk material ε' values with the decrease of the frequency in the low frequency region as demonstrated earlier.[62,63] In contrast to the PEO, the increase in ε' values of pristine PVDF film with the decrease of frequency in the AF-region is very small, which reveals that there is insignificant contribution of IP effect and the dispersion is found almost frequency-independent over the frequency range, *i.e.*, 20 Hz-1 MHz. Further, the ε'' and $\tan\delta$ values of PEO film are relatively very high as compared to that of the PVDF film at lower frequencies, and its $\tan\delta$ spectrum exhibits a dielectric relaxation peak around 20 kHz which is associated to its chain segmental dynamics as reported in the earlier studies.[62,63,88] Because of these differences in the dielectric polarization processes of the PVDF and the PEO films, the dielectric study of their blends is expected to be interesting.

For the PVDF/PEO blend films, the low frequency ε' values enhance with the increase of PEO amount in the blend films, whereas they gradually decrease in the high frequency region which can be read from the enlarged view of the ε' spectra given in Figure 7. This finding confirms that the IP effect contri-

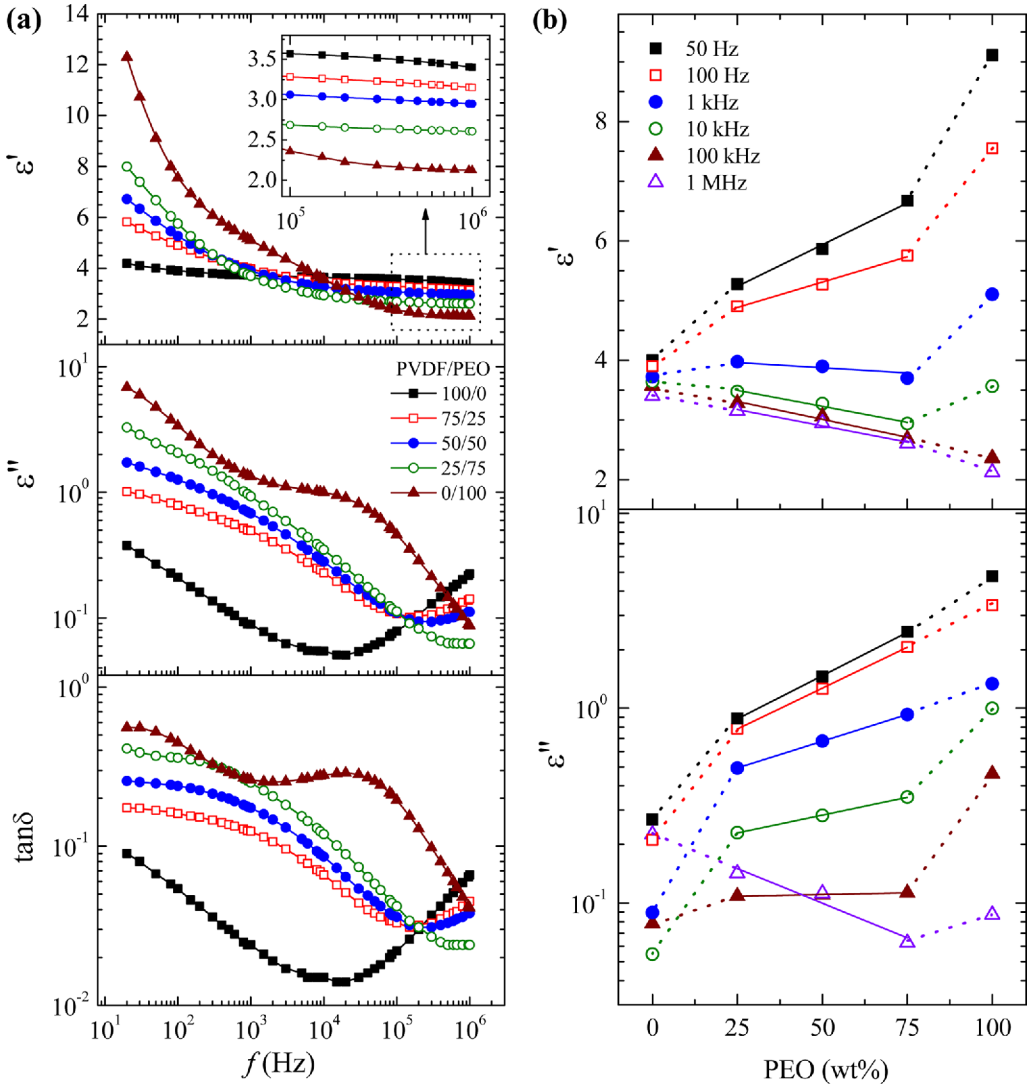

Figure 7. (a) Complex dielectric permittivity (real part ε' and imaginary part ε'') and loss tangent tanδ spectra of the PVDF film, PVDF/PEO blend films, and the PEO film at 27 °C. The inset shows the enlarged view of ε' values in 100 kHz to 1 MHz range. (b) The variation of ε' and ε'' values with increase of PEO concentration in the blend films at fixed frequencies are marked by solid lines for the blend films, which were connected to those of the pristine polymers by dotted lines.

bution dominates over the dipolar polarization of these polymers blends at low frequencies but at high frequencies their ε' values are simply governed by the weight fraction additive mixing rule which holds for the composite dielectric materials. This effect also reflects in the ε'' spectra of these PVDF/PEO blend films (Figure 7). Further, the PEO chain segmental relaxation process peaks in the tanδ spectra of these blend films are not noticeable over this experimental frequency range, at the ambient temperature.

Figure 7(b) shows the variation of ε' values of the PVDF/PEO blend films with a change of PEO concentration (wt%) at different fixed frequencies. This figure confirms that the ε' decreases linearly with the increase of PEO concentration in the blends at 10 kHz, 100 kHz, and 1 MHz frequencies which is applicable to all the frequencies lying between these limiting values. Further, the rate of increment of the ε' values at these frequencies is almost the same. This finding confirms that the ε' value can be tuned in the range 2 to 4 at the higher radio frequencies with the change of the compositional ratio of the PVDF/PEO blend. But at lower audio frequencies (50 Hz and 100 Hz in Figure 7(b)) the ε' values linearly enhance with the increase of PEO concentration in these blends and also with different rates of increment. These results infer that the presence of PEO in the PVDF matrix greatly enhances the IP effect and its contribution in the low frequency dielectric polarization processes, and hence the IP effect at low frequencies can be controlled by suitably adjusting the compositional ratio of these polymers in their blend films. Further, from Figure 7(b) it was noticed that the ε' values at 1 kHz are almost independent of the blend compositional ratio. In regards to the confirmation of the dependence of ε'' values on the compositional ratio of the PVDF and PEO in their blend films, Figure 7(b) is plotted. It is observed from the figure that the ε'' values on the logarithmic scale enhance linearly with the increase of PEO amount in the blends at lower frequencies, whereas at 10 kHz and 100 kHz, these values are independent of compositional ratio, but at 1 MHz the ε'' decrease with the increase of PEO concentration. The different behaviour of these compositional ratio-dependent ε' and ε'' values of the PVDF/PEO blend

films at various frequencies suggests their numerous dielectric applications tunable with compositional ratio of the blend and/or frequency of electric field used for the excitation of these materials.

3.6. Electric modulus spectra

The complex electric modulus (real part M' and imaginary part M'') spectra of the PVDF/PEO blend films are shown in Figure 8. These spectra are derived by transforming the frequency-dependent complex dielectric permittivity data of these materials. Because of the inverse relationship between the electric modulus and dielectric permittivity, the spectra of electric modulus remain free from electrode polarization (EP) effect, electrode/dielectric contact of the sample holder during the measurements, and also from the type of electrode material and their geometry, and therefore the electric modulus function is commonly preferred for the analysis of relaxation processes in the composite materials.[13,27,57,62-65,88-92] Figure 8 shows that the M' (f) values of pure PVDF film have a little enhancement with the increase of frequency from 20 Hz to 1 MHz which is expected because of slow decrease in its ε' (f) values. Similarly, the M' (f) values of the PVDF/PEO blend films and also for the pure PEO film initially enhance by a large amount with the increase of frequency, and finally approach steady state at high frequencies which are also expected according to their ε'(f) values (Figure 7). The non-zero M' values (*i.e.*, the continuous increasing behaviour of the spectra up to 10 kHz) of the PVDF/PEO blend films reveal that the observed ε' spectra of these materials are free from the electrode polarization effect as demonstrated earlier for the polymeric

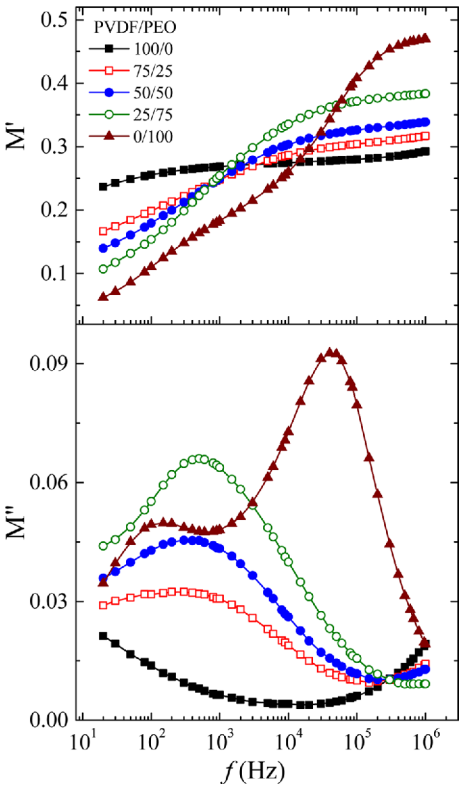

Figure 8. Complex electric modulus (real part M' and imaginary part M'') spectra at 27 °C of the PVDF film, PVDF/PEO blend films, and the PEO film.

nanodielectrics.[57,62,63] Further, from the M' spectra, one can note that there is a decrease in M' values at a fixed frequency in the low frequency-region as the PEO content in the PVDF/PEO blend films enhances, whereas it shows an inverse trend in the high frequency region.

Figure 8 shows that the M'' spectrum of pristine PEO exhibits a sharp and intense relaxation peak around 50 kHz, and a relatively less intense peak around 100 Hz which are attributed to the polymer chain segmental motion and the IP relaxation processes, respectively.[62] There is no relaxation process in the pure PVDF film over the frequency range 20 Hz to 1 MHz at room temperature which is in agreement with the earlier results.[13,27,93] It is reported that the PVDF relaxation peak is exhibited at ~3 Hz at 30 °C, whereas it appeared at about 6 kHz when the film temperature is 100 °C.[13] Further, the PVDF/PEO blend films exhibit relaxation peak in the frequency range 100 Hz to1 kHz, and the peak intensity gradually enhances and its broadness reduces with the increase of PEO amount in these blend films. The relatively more broadness of the relaxation peak for the PVDF-rich blend film indicates the highly asymmetrical distribution of its relaxation process. Further, a small shift of the peak towards higher frequency side is also noted with the increase of PEO concentration in the PVDF/PEO blend films. This relaxation peak of the blends can be assigned to the PEO chain segmental dynamics probably confined in the PVDF crystals. The modulus relaxation time τ_M of this dynamical process is determined from the M'' peak frequency f_{max} value using the relation $\tau_M=1/\omega_{max}$ where $\omega_{max}=2\pi f_{max}$, and the obtained τ_M values of the blend films are recorded in Table 5. The τ_M values of the PVDF/PEO blend films are found about two orders of magnitude higher than that of the pristine PEO film which firmly confirms the confined dynamics of PEO structures in the PVDF matrix as suggested earlier.[53]

3.7. AC conductivity spectra

The spectra of real part $\sigma'=\omega\varepsilon_0\varepsilon''$ and imaginary part $\sigma''=\omega\varepsilon_0\varepsilon'$ of the ac electrical conductivity for the PVDF/PEO blend films over the frequency range 20 Hz to 1 MHz, at 27 °C, are depicted in Figure 9. It is observed that the $\sigma'(f)$ increase non-linearly with the increase of frequency, whereas the $\sigma''(f)$ exhibit a linear behaviour over the entire frequency range. The frequency-dependent σ' values of the PVDF films and the shape of its σ' spectrum at room temperature are also found consistent with earlier studies.[7,19,60,83,87,91] Further, it is observed that the σ' values of all these polymer blend films also vary linearly in the lower frequency range, *i.e.*, 20 Hz to 1 kHz. Therefore, by using the

Table 5. Values of electric modulus relaxation time τ_M and the dc electrical conductivity σ_{dc} at 27 °C of the pure PVDF film, PVDF/PEO blend films, and the pure PEO film

Polymer films	τ_M ($\times10^{-5}$ s)	σ_{dc} ($\times10^{-12}$ S/cm)
Pure PVDF	-	0.66
75 PVDF/25 PEO	65.5	1.03
50 PVDF/50 PEO	44.7	2.09
25 PVDF/75 PEO	31.7	4.88
Pure PEO	0.37	14.02

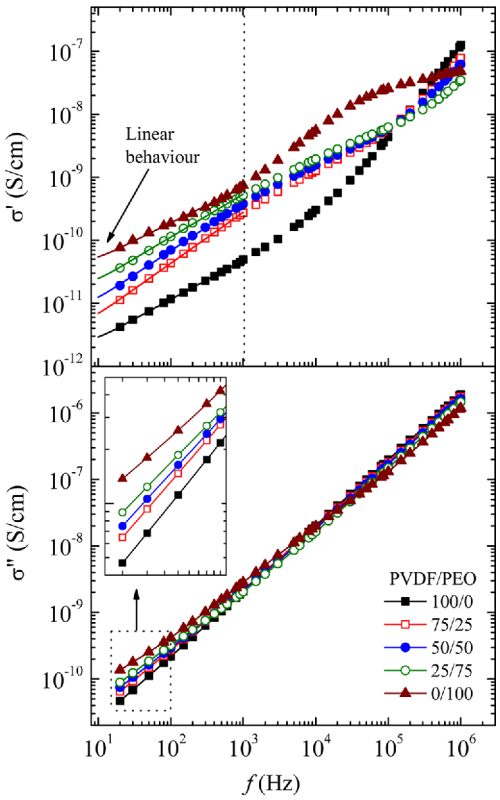

Figure 9. The ac electrical conductivity (real part σ' and loss part σ) spectra at 27 °C of the PVDF film, PVDF/PEO blend films, and the PEO film. Inset shows the enlarged view of low frequency σ'' spectra of the films. The solid lines in σ' spectra represent the linear fit of the low frequency data.

straight line fit of the linear portions of these σ' spectra, the dc electrical conductivity σ_{dc} values of the PVDF/PEO blend materials were determined and the same are recorded in Table 5. It can be noted from Table 5 that the σ_{dc} value of pure PVDF film is 6.6×10^{-13} S/cm which is very low and it increases with the increase of PEO concentration in the PVDF/PEO blend films. Further, from Table 5, it can be noted that there is a difference of about two orders of magnitude between the conductivities of the pure PVDF film and the pure PEO film, at 27 °C. This result is interesting in regards to design the conductivity-tunable flexible dielectric based on the PVDF/PEO blend.

Figure 10 illustrates the τ_M and σ_{dc} versus PEO (wt%) plots for the PVDF/PEO blend films, at 27 °C. It can be noted that on the logarithmic scale, the σ_{dc} values exhibit a non-linear increase of about two orders of magnitude with the increase of PEO concentration in the blend films over the entire concentration range, whereas the τ_M values exhibit a linear decrease within one order of magnitude for the PVDF/PEO blend films. Further, it is noted that the τ_M values of these PB films are about two orders of magnitude higher as compared to that of the pristine PEO film. These results confirm that the PVDF/PEO blend films can be used as dc electrical conductivity- and the structural dynamics-tunable dielectric materials by simply varying their compositions.

3.8. Temperature-dependent dielectric properties

The effect of temperature on the dielectric dispersion of 50 PVDF/

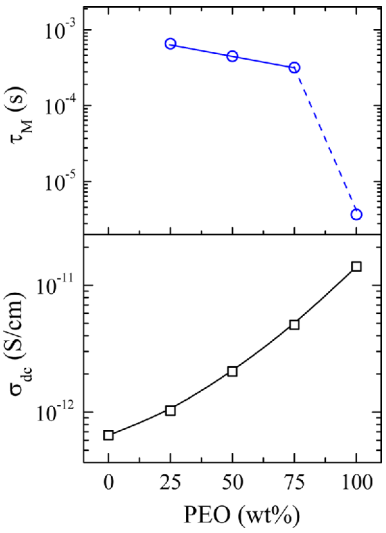

Figure 10. The plots of relaxation time τ_M and dc electrical conductivity σ_{dc} versus concentration of PEO (wt%) at 27 °C for the PVDF/PEO blend films.

50 PEO blend film has been investigated as a representative sample for the PVDF/PEO blend films. Figure 11(a) shows that the ε' values of the blend film have a small increase at high frequencies but there is a significant increase of ε' values at low frequencies with the increase of temperature from 27 to 60 °C. Further, the tanδ values also have some increase below 100 kHz with the increase of temperature of the film but there is no distinguishable relaxation peak in these tanδ spectra. Figure 11(b) shows the M'' spectra of the 50 PVDF/50 PEO blend film at different temperatures. A sharp and intense relaxation peak appeared in the M'' spectra has a gradual increase in its magnitude and shifts towards higher frequency side with the increase of temperature of the film. The enhancement in ε' value and the decrease of relaxation time $\tau_M=1/2\pi f_{max}$ with the increase of temperature of the PB film confirm its thermally activated dielectric polarization and structural dynamics as mostly observed in the PNC materials.[13,57,75,93] Figure 11(c) shows the Arrhenius plot of τ_M values which fairly obeys the exponential relation $\tau_M=\tau_0 \exp(E_\tau/k_BT)$ from which the relaxation time activation energy E_τ is determined. The E_τ value for this blend film is found 0.23 eV which is very low confirming the suitability of the PVDF/PEO blend film as a host matrix for the preparation of solid polymer electrolytes.

4. Conclusions

This paper reports the relative fraction of the crystal phases of PVDF film and their alteration due to its blending with PEO. The detailed morphology, degree of crystallinity, chemical composition, and the dielectric and electrical properties of the various compositional ratio PVDF/PEO blend films prepared by solution casting have been investigated. The PVDF film contains mainly the α- and β-phases with its 37% total degree of crystallinity which further enhances non-linearly with the increase of PEO concentration in the blends. The simple fractional relations for the determination of the relative fraction of the β-phase in the PVDF/PEO blend films with respect to that of the pristine PVDF

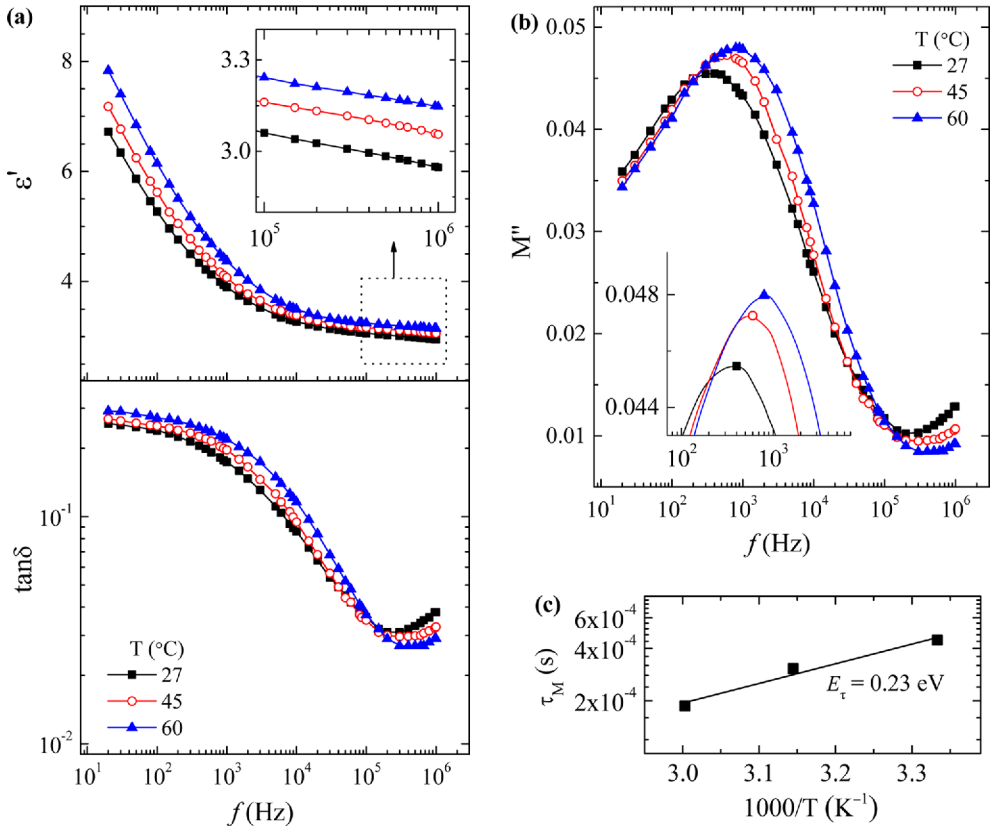

Figure 11. (a) The real part of the complex dielectric permittivity ε' and loss tangent tanδ spectra of the 50 PVDF/50 PEO blend film, (b) the imaginary part M'' of complex electric modulus spectra at different temperatures, and (c) the Arrhenius plot of the relaxation time.

film have been proposed which are based on the areas and intensities of the crystalline peaks in their XRD patterns. The 75 PVDF/25 PEO blend has about 50% β-phase fraction, and it is relatively very small (12.5%) for the 25 PVDF/75 PEO blend film. The results on the dielectric properties confirmed that the ε' values of the PVDF/PEO blend films at radio frequencies (20 kHz-1 MHz) can be tuned in the range 2 to 4 with the adjustment of these blended polymers compositional ratio. The lower audio frequency range ε' values of the blend films are relatively high which are predominantly governed by the large contribution of the interfacial polarization effect. The PEO chain segmental dynamics is found greatly hindered in the blend films because of the PEO chains confinement in the matrix of PVDF crystallites. The dc electrical conductivity of these blend materials enhances from 6.6×10^{-13} to 1.4×10^{-11} S/cm with the increase of PEO contents in the PVDF/PEO blend, which also confirm the conductivity-tunable behaviour of these blend films to be used as flexible dielectric materials. The temperature-dependent dielectric properties of the 50 PVDF/50 PEO blend film confirm that the blend has thermally activated behaviour of dielectric polarization and the PEO chain segmental dynamics, and the relaxation activation energy of this blend is found significantly low (0.23 eV). The polymer compositional ratio-dependent dielectric and electrical behaviour of these PVDF/PEO blend films has been explained in detail for exploring their suitability as dielectric materials for the advances in flexible electronics and energy storing/harvesting devices.

References

(1) P. Atorngitjawat, *Macromol. Res.*, **25**, 391 (2017).
(2) P. Martins, A. C. Lopes, and S. Lanceros-Mendez, *Prog. Polym. Sci.*, **39**, 683 (2014).
(3) M. Li, I. Katsouras, C. Piliego, G. Glasser, I. Lieberwirth, P. W. M. Blom, and D. M. de Leeuw, *J. Mater. Chem. C*, **1**, 7695 (2013).
(4) Prateek, V. K. Thakur, and R. K. Gupta, *Chem. Rev.*, **116**, 4260 (2016).
(5) W. Xia and Z. Zhang, *IET Nanodielectr.*, **1**, 17 (2018).
(6) R. Ding, L. Gong, M. Li, S. Chen, S. Zhan, X. Sun, C. Zhang, and T. Shao, *Macromol. Res.*, **26**, 965 (2018).
(7) Y. Li, D. Zhang, S. Wang, Y. Zhan, J, Yin, X. Tao, X. Ge, S. C. Tjong, H.-Y. Liu, and Y. W. Mai, *Compos. Sci. Technol.*, **171**, 152 (2019).
(8) X. Bi, S. Song, and S. Sun, *Macromol. Res.*, **25**, 1163 (2017).
(9) E. Kar, N. Bose, B. Dutta, S. Banerjee, N. Mukherjee, and S. Mukherjee, *Energy Convers. Manag.*, **184**, 600 (2019).
(10) B. Jiang, J. Iocozzia, L. Zhao, H. Zhang, Y.-W. Harn, Y. Chen, and Z. Lin, *Chem. Soc. Rev.*, **48**, 1194 (2019).
(11) F. S. Al-Hazmi, D. M. de Leeuw, A. A. Al-Ghamdi, and F. S. Shokr, *Curr. Appl. Phys.*, **17**, 1181 (2017).
(12) B. Jiang, X. Pang, B. Li, and Z. Lin, *J. Am. Chem. Soc.*, **137**, 11760 (2015).
(13) C. Tsonos, H. Zois, A. Kanapitsas, N. Soin, E. Siores, G. D. Peppas, E. C. Pyrgioti, A. Sanida, S. G. Stavropoulos, and G. C. Psarras, *J. Phys. Chem. Solids*, **129**, 378 (2019).
(14) A. Jain, K. J. Prashanth, A. K. Sharma, A. Jain, and P. N. Rashmi, *Polym. Eng. Sci.*, **55**, 1589 (2015).
(15) A. Joseph and G. M. Joshi, *J. Mater. Sci. Mater. Electron.*, **29**, 4749 (2018).
(16) J. P. Jung, J.-S. Kim, T.-S. Han, and J. H. Kim, *Macromol. Res.*, **25**, 365 (2017).
(17) R. Barstugan, M. Barstugan, and I. Ozaytekin, *Compos. Part B*, **158**, 141 (2019).
(18) P. Thakur, A. Kool, N. A. Hoque, B. Bagchi, F. Khatun, P. Biswas, D. Brahma, S. Roy, S. Banerjee, and S. Das, *Nano Energy*, **44**, 456 (2018).

(19) S. Dash, R. N. P. Choudhary, and M. N. Goswami, *J. Alloys Compd.*, **715**, 29 (2017).
(20) N. An, H. Liu, Y. Ding, M. Zhang, and Y. Tang, *Appl. Surf. Sci.*, **257**, 3831 (2011).
(21) M. Choi, G. Murillo, S. Hwang, J. W. Kim, J. H. Jung, C.-Y. Chen, and M. Lee, *Nano Energy*, **33**, 462 (2017).
(22) A. M. Ismail, M. I. Mohammed, and S. S. Fouad, *J. Mol. Struct.*, **1170**, 51 (2018).
(23) S. Huang, G. Tang, H. Huang, X.-G. Wu, P. Zhou, L. Zou, L. Xie, J. Deng, X. Wang, H. Zhong, and J. Hong, *Sci. Bull.*, **63**, 1254 (2018).
(24) G. Prasad, P. Sathiyanathan, A. A. Prabu, and K. J. Kim, *Macromol. Res.*, **25**, 981 (2017).
(25) G. Melilli, D. Lairez, D. Gorse, E. Garcia-Caurel, A. Peinado, O. Cavani, B. Boizot, and M.-C. Clochard, *Radiat. Phys. Chem.*, **142**, 54 (2018).
(26) S. Wolff, F. Jirasek, S. Beuermann, and M. Türk, *RSC Adv.*, **5**, 66644 (2015).
(27) P. Xu, W. Fu, Z. Cui, and Y. Ding, *Appl. Phys. Lett.*, **112**, 063904 (2018).
(28) W. Xia, M. Xie, X. Feng, L. Chen, and Y. Zhao, *Macromol. Res.*, **26**, 1225 (2018).
(29) L. Zhou, N. Wu, Q. Cao, B. Jing, X. Wang, Q. Wang, and H. Kuang, *Solid State Ionics*, **249-250**, 93 (2013).
(30) S. V. Kuppu, A. R. Jeyaraman, P. K. Guruviah, and S. Thambusamy, *Curr. Appl. Phys.*, **18**, 619 (2018).
(31) X. Li, Y. Chen, X. Hu, Y. Zhang, and L. Hu, *J. Membr. Sci.*, **471**, 118 (2014).
(32) X. Lin, L. Fan, D. Ren, Z. Jiao, P. Coates, and W. Yang, *Compos. Part B: Eng.*, **114**, 58 (2017).
(33) M. Muthuvinayagam and C. Gopinathan, *Polymer*, **68**, 122 (2015).
(34) F.-C. Chiu and S.-C. Yeh, *Polym. Testing*, **45**, 114 (2015).
(35) S. Choudhary and R. J. Sengwa, *Mater. Chem. Phys.*, **142**, 172 (2013).
(36) Z. Xue, D. He, and X. Xie, *J. Mater. Chem. A*, **3**, 19218 (2015).
(37) A. Arya and A. L. Sharma, *J. Phys. D. Appl. Phys.*, **50**, 443002 (2017).
(38) F. Wang, L. Li, X. Yang, J. You, Y. Xu, H. Wang, Y. Ma, and G. Gao, *Sustainable Energy Fuels*, **2**, 492 (2018).
(39) S. Janakiraman, A. Surendran, S. Ghosh, S. Anandhan, and A. Venimadhav, *Mater. Res. Exp.*, **6**, 035303 (2018).
(40) I. S. Elashmawi, N. H. Elsayed, and F. A. Altalhi, *J. Alloys Compd.*, **617**, 877 (2014).
(41) R. Rathika and S. A. Suthanthiraraj, *Macromol. Res.*, **24**, 422 (2016).
(42) P. Chen, X. Liang, J. Wang, D. Zhang, S. Yang, W. Wu, W. Zhang, X. Fan, and D. Zhang, *J. Sol-Gel Technol.*, **81**, 850 (2017).
(43) S. K. Patla, R. Ray, K. Asokan, and S. Karmakar, *J. Appl. Phys.*, **123**, 125102 (2018).
(44) D. S. Song, H.-Y. Cho, B.-R. Yoon, J. Y. Jho, and J. H. Park, *Macromol. Res.*, **25**, 135 (2017).
(45) R. Rathika and S. A. Suthanthiraraj, *J. Mater. Sci. Mater. Electron.*, **29**, 19632 (2018).
(46) F. Deng, X. Wang, D. He, J. Hu, C. Gong, Y. S. Ye, X. Xie, and, Z. Xue, *J. Membr. Sci.*, **491**, 82 (2015).
(47) Y. Yang, J. Zhang, C. Zhou, S. Wu, S. Xu, W. Liu, H. Han, B. Chen, and X. Zhao, *J. Phys. Chem. B*, **112**, 6594 (2008).
(48) S. K. Patla, M. Mukhopadhyay, R. Ray, P. Maiti, A. K. Mukhopadhyay, D. Sen, and K. Asokan, *Ionics*, **25**, 2159 (2019).
(49) S. Ganesan, P. Karthika, R. Rajarathinam, M. Arthanareeswari, V. Mathew, and P. Maruthamuthu, *Solar Energy*, **135**, 84 (2016).
(50) M. Mohamadi, H. Garmabi, and M. Papila, *Macromol. Res.*, **24**, 698 (2016).
(51) M. Mohamadi, H. Garmabi, and M. Papila, *Polym. Bull.*, **74**, 2117 (2017).
(52) M. N. Tamaño-Machiavello, C. M. Costa, J. Molina-Mateo, C. Torregrosa-Cabanilles, J. M. M. Dueñas, S. N. Kalkura, S. Lanceros-Mendez, R. S. I. Serra, and J. L. G. Ribelles, *Mater. Today Commun.*, **4**, 214 (2015).
(53) M. N. Tamaño-Machiavello, C. M. Costa, F. J. Romero-Colomer, J. M. M. Dueñas, S. Lanceros-Mendez, and J. L. G. Ribelles, *J. Polym. Sci.: Polym. Phys.*, **56**, 588 (2018).
(54) I. S. Elashmawi and L. H. Gaabour, *Results Phys.*, **5**, 105 (2015).
(55) F. H. Abd El-kader, N. A. Hakeem, R. S. Hafez, and A. M. Ismail, *J. Inorg. Organomat. Polym. Mater.*, **28**, 1037 (2018).
(56) R. J. Sengwa, S. Choudhary, and P. Dhatarwal, *Adv. Compos. Hybrid Mater.*, **2**, 162 (2019).
(57) S. Choudhary and R. J. Sengwa, *Curr. Appl. Phys.*, **18**, 1041 (2018).
(58) S. F. Mendes, C. M. Costa, V. Sencadas, J. S. Nunes, P. Costa, R. G. Jr., and S. L. Méndez, *Appl. Phys. A*, **96**, 899 (2009).
(59) A. Jain, S. J. Kumar, M. R. Kumar, A. S. Ganesh, and S. Srikanth, *Mech. Adv. Mater. Struct.*, **21**, 181 (2014).
(60) I.-H. Kim, D. H. Baik, and Y. G. Jeong, *Macromol. Res.*, **20**, 920 (2012).
(61) P. Xu, W. Fu, X. Luo, and Y. Ding, *Mater. Lett.*, **206**, 60 (2017).
(62) R. J. Sengwa and S. Choudhary, *J. Alloys Compd.*, **701**, 652 (2017).
(63) S. Choudhary and R. J. Sengwa, *J. Polym. Res.*, **24**, 54 (2017).
(64) A. M. Abdelghany, E. M. Abdelrazek, S. I. Badr, and M. A. Morsi, *Mater. Design*, **97**, 532 (2016).
(65) S. Choudhary and R. J. Sengwa, *J. Inorg. Organomet. Polym. Mater.*, **29**, 592 (2018).
(66) P. Dhatarwal, R. J. Sengwa, and S. Choudhary, *SN Appl. Sci.*, **1**, 112 (2019).
(67) X. Cai, T. Lei, D. Sun, and L. Lin, *RSC Adv.*, **7**, 15382 (2017).
(68) S. R. A. Karim, L. H. Sim, C. H. Chan, and H. Ramli, *Macromol. Symp.*, **354**, 374 (2015).
(69) K. Kiran Kumar, M. Ravi, Y. Pavani, S. Bhavani, A. K. Sharma, and V. V. R. Narasimha Rao, *J. Membr. Sci.*, **454**, 200 (2014).
(70) B. Jinisha, K. M. Anilkumar, M. Manoj, V. S. Pradeep, and S. Jayalekshmi, *Electrochim. Acta*, **235**, 210 (2017).
(71) A. Rajeh, M. A. Morsi, and I. S. Elashmawi, *Vacuum*, **159**, 430 (2019).
(72) S. Cho, J. S. Lee, and J. Jang, *ACS Appl. Mater. Interfaces*, **7**, 9668 (2015).
(73) Q. Fu, G. Lin, X. Chen, Z. Yu, R. Yang, M. Li, X. Zeng, and J. Chen, *Energy Technol.*, **6**, 144 (2018).
(74) K. Deshmukh, M. B. Ahamed, R. R. Deshmukh, S. K. K. Pasha, K. K. Sadasivuni, D. Ponnamma, and M. Al-Ali AlMaadeed, *J. Mater. Sci. Mater. Electron.*, **28**, 559 (2017).
(75) M. S. Gaur, A. P. Indolia, A. A. Rogachev, and A. V. Rahachou, *J. Therm. Anal. Calorim.*, **122**, 1403 (2015).
(76) X.-J. Zha, J.-H. Pu, L.-F. Ma, T. Li, R.-Y. Bao, L. Bai, Z.-Y. Liu, M. B. Yang, and W. Yang, *Compos. Part A*, **105**, 118 (2018).
(77) H. Li, Z. Chen. L. Liu, J. Chen, M. Jiang, and C. Xiong, *Compos. Sci. Technol.*, **121**, 49 (2015).
(78) F. Mao, Z. Shi, J. Wang, C. Zhang, C. Yang, and M. Huang, *Adv. Compos. Hybrid Mater.*, **1**, 548 (2018).
(79) P. Wang, P. Xu, Y. Zhou, Y. Yang, and Y. Ding, *Eur. Polym. J.*, **99**, 58 (2018).
(80) W. Zhou, Y. Gong, L. Tu, L. Xu, W. Zhao, J. Cai, Y. Zhang, and A. Zhou, *J. Alloys Compd.*, **693**, 1 (2017).
(81) X. Zhang, S. Zhao, F. Wang, Y. Ma, L. Wang, D. Chen, C. Zhao, and W. Yang, *App. Surf. Sci.*, **403**, 71 (2017).
(82) N. Jahan, F. Mighri, D. Rodrigue, and A. Ajji, *Appl. Clay Sci.*, **152**, 93 (2018).
(83) Y. Gong, W. Zhou, Z. Wang, L. Xu, Y. Kou, H. Cai, X. Liu, Q. Chen, and Z.-M. Dang, *J. Mater. Sci. Technol.*, **34**, 2415 (2018).
(84) W. Zhou, L. Xu, L. Jiang, J. Peng, Y. Gong, X. Liu, H. Cai, G. Wang, and Q. Chen, *J. Alloys Compd.*, **710**, 47 (2017).
(85) Y. Zhu, P. Jiang, Z. Zhang, and X. Huang, *Chinese Chem. Lett.*, **28**, 2027 (2017).
(86) X. Hu, K. Yi, J. Liu, and B. Chu, *Energy Technol.*, **6**, 849 (2018).
(87) Z. Wang, T. Wang, Y. Xiao, W. Nian, and H. Chen, *Ceram. Int.*, **44**, S181 (2018).
(88) S. Choudhary and R. J. Sengwa, *Polym. Bull.*, **72**, 2591 (2015).
(89) J. Yu, W. Wu, D. Dai, Y. Song, C. Li, and N. Jiang, *Macromol. Res.*, **22**, 19 (2014).
(90) H. Rekik, Z. Ghallabi, I. Royaud, M. Arous, G. Seytre, G. Boiteux, and A. Kallel, *Compos. Part B*, **45**, 1199 (2013).
(91) C. Tsonos, C. Pandis, N. Soin, D. Sakellari, E. Myrovali, S. Kripotou, A. Kanapitsas, and E. Siores, *Express Polym. Lett.*, **9**, 1104 (2015).
(92) S. Choudhary, *J. Mater. Sci. Mater. Electron.*, **29**, 10517 (2018).
(93) D. He, Y. Wang, L. Zhang, S. Song, and Y. Deng, *Compos. Sci. Technol.*, **159**, 162 (2018).

